




A potential optical sensor based on nanostructured silicon

Shahzad Ahmed^{1,*} , Arshiya Ansari¹, Moin Ali Siddiqui¹, Afzal Khan^{2,*}, and Pranay Ranjan^{1,*}

¹ Department of Metallurgical and Materials Engineering, Indian Institute of Technology Jodhpur, Jodhpur, Rajasthan 342037, India

² State Key Laboratory of Silicon Materials, School of Materials Science and Engineering, Zhejiang University, Hangzhou 310027, China

Received: 30 January 2023

Accepted: 25 February 2023

Published online:

14 March 2023

© The Author(s), under exclusive licence to Springer Science+Business Media, LLC, part of Springer Nature 2023

ABSTRACT

Silicon (Si); the most abundant raw material on the earth's crust upholds a promising future in the silicon or electronic industry. However, the intrinsic indirect bandgap (1.12 eV), limits its usage in optoelectronics devices due to the passage of the infrared spectrum. Herein, we have structurally modified the Si structure into a nanostructured material like porous silicon (PS) for application in optoelectronic devices. In order to make PS structures, n-type monocrystalline Si was anodized in an ethanoic-HF solution. The average diameter of the pores created by anisotropic electrochemical etching with fixed time and current density was determined to be around 250 nm. The PS demonstrated a direct bandgap and an energy gap of 1.73 eV. The obtained PS-based device's photoresponse was investigated at various laser irradiation wavelengths. The best response sensitivity of 11.18% was noted at a wavelength of 786 nm, thus, promising to be a potential material for visible range photodetectors.

1 Introduction

Substances with the necessary transducer qualities must be carefully chosen for the creation and manufacture of the sensor module. Due to their distinctive physicochemical properties with respect to their bulk forms, including their great surface-by-volume ratio, tiny dimension, optical sensitivity, light absorption, and thermal and electrical conductivity,

nanostructured substances have become increasingly popular in many uses [1, 2] which include pressure sensors, chemical sensors, gas sensors, optical sensors [3], etc. Due to its notable optical and physical characteristics, porous silicon (PS), one of the numerous readily available nanostructure-based materials (such as quantum dots (QDs), metallic nanoparticles, and carbon nanotubes), has exceptional potential for utilization in a number of scientific domains such as sensors, drug delivery, and optical switching. While

Shahzad Ahmed and Arshiya Ansari have contributed equally to this work.

Address correspondence to E-mail: p22mt007@iitj.ac.in; afzalkhan@zju.edu.cn; pranay.ranjan@iitj.ac.in

porous silicon was unintentionally found by Uhlir in 1956 while conducting electrochemical testing [4], this material gained special recognition in 1990 when Canham identified the material's inherent photoluminescence (PL) at room temperature. According to the consistent variety of scientific articles on PS-based sensors reported every year in peer-reviewed publications, it has been an active topic for research investigations since the preliminary tests on PS as a sensor tool two decades ago. The PS substance has air-filled cavities along with a large surface area (up to $800 \text{ m}^2 \text{ g}^{-1}$); these intriguing features, along with the substance's adaptable surface chemical alteration, controllable feature dimensions, biodegradability, biocompatibility, and photoluminescence, render it a desirable optical transducer.

PS exhibits distinctive luminescent characteristics with a high density of nanostructured cavities and columns on the surface owing to quantum confinement effects in nanocrystals [5–7]. Additionally, it has a special negative differential conductance property. The vast surface region, great sensitivity, and range of optical transduction potential of PS, such as variation in fluorescence or reflectance (interferometric detection) [8], have led to substantial research into its potential as an optical sensing device.

Electrochemical etching is a typical method for fabricating PS platforms since it doesn't call for overpriced machinery and ensures high reproducibility. This method allows for precise customization of the material's optical responsiveness and pore diameter. Additional porous materials, including porous titania or porous alumina, are often difficult to tune [9]. Furthermore, an electrochemical-based etching procedure involves placing a Si wafer in a cell, submerging it in an etching solution that contains fluoride, and then applying current to the system. An electrode made of platinum serves as the cathode and Si serves as the anode in the typical electrochemical process. Different porosity architectures may be produced based on various factors, including the etching solution's content, the doping of Si, and the magnitude of current density. Thus, the current density plays a significant influence on the pore dimension that results. This fact was effectively used to regulate the pore dimension in the porous material that is parallel to the Si surface. The development process of the holes, where the dissolution of Si nearly entirely happens at the hole tips, is directly related to the required high reflectivity of the Si

surface. The anodization etching approach, which is the most widely used, is one of many production techniques [10] developed for the manufacture of PS.

BaTiO₃ [11] has been explored in other papers as a photodetector [12]. Porous structures have also been used in various applications, such as gas sensing [13] and electrochemical sensing [14]. On the other side, magnetic nanoparticles [15] were also used for UV photodetection [16]. A hydrogel-based [17] photodetection device [18] was used in a different investigation. A graphene sheet [19–23] produced by CVD [24] was also used to examine the photodetection [25–27]. Additionally, the electrochemical approach [14] is used to create the porous structure since it is simple to use and affordable [28].

Additionally, Hadi et al. [29] showed a solution cast and electrochemically manufactured polystyrene/PS heterojunction photodetector. In stark contrast to the currently available Si photodetectors, Jang et al. [30] developed graphene/WS₂/PS heterostructure photodetectors with such a wide-band photoresponse in the visible region. The authors have also covered the simulation approach and system design for photodetector [31] and other applications [32].

Thus, as a continuation of our earlier work [33], we have demonstrated a better outcome by adjusting the parameters, such as current density and etching duration, in this study. Here, we produced nanostructured PS substances and tuned the bandgap of n-type Si using an economical photo-assisted anisotropic electrochemical etching approach. Different illumination sources were employed to successfully boost the sensitivity of the optical sensing action of a device realized on a nanostructured PS substance. The sensitivity was discovered to be 11.18% when light with a wavelength of 786 nm was being used. As a result, the current work will help in the development of PS-based photodetectors for optoelectronics in the visible region, particularly in the red-light spectrum.

2 Materials and methods

Without additional purification, all reagents were used as received. Aluminum paste, acetone ((CH₃)₂CO), hydrogen fluoride (HF), ethanol (C₂H₅OH), and n-type silicon (100) wafers were utilized for the

experiment. The substances were all bought from Central Drug House (CDH) and related companies.

2.1 Apparatus and measurements

With an electrochemical test measuring apparatus (Solartron analytical 1280), etching was carried out in galvanostatic mode. The surface morphology of PS materials was investigated using field emission scanning electron microscopy (FESEM) (Hitachi). Using the customized Olympus integrated laser system Raman spectroscopy, the Raman spectra were acquired. PL experiments were carried out in the 500–800 nm wavelength range using the PerkinElmer (Lambda 950). We collected FTIR readings using the Jasco FT-IR. The manufactured optical sensor was placed in a two-probe chamber (Linkam, UK) and electrical signals were analyzed using the Keithley SCS 4200 framework to study the photoresponses.

2.2 Experimental

In our experiment, the Si wafers had a resistivity of 1–10 $\Omega\text{-cm}$ and a surface density of 6.78×10^{14} atoms cm^{-2} . The silicon wafer was first hydrothermally cleaned for 30 min in acetone and ethanol in succession in a vacuum oven to remove unwanted dust and impurities. The electrochemical etching process was used to create the nano-dimensioned PS architecture. Figure 1 illustrates how DC anodization was carried out in an electrochemical cell employing a two-electrode arrangement. The Si wafer's forepart was protected by a fluorosilicone O-ring, and its rear part was covered in a silver paste that allowed for an Ohmic connection between the wafer and an aluminum plate that served as an anode. The Teflon cell had a 40 mL volume. The cathode used was a platinum wire. Electrolyte mixtures comprised an identical volume ratio of HF to ethanol were called etchants. Due to their strong electronegative properties, fluoride ions facilitated the formation of holes on the Si surface. DC anodization was performed at the standard room temperature for a predetermined 18 min at a current density of 32 mA cm^{-2} . The capture of a hole causes the n-type Si etching to begin. When the Si is exposed to a laser beam during laser-guided etching, the formation of electron/hole pairs is facilitated. The forepart of the wafer was therefore illuminated with an illumination source to produce electrical holes. As long as the bias voltage remained under breakdown,

there was no actual etching of n-type Si without illumination. Along with the output, Fig. 1 also depicts the design of the device's electrical measurements using different light wavelengths.

3 Results and discussion

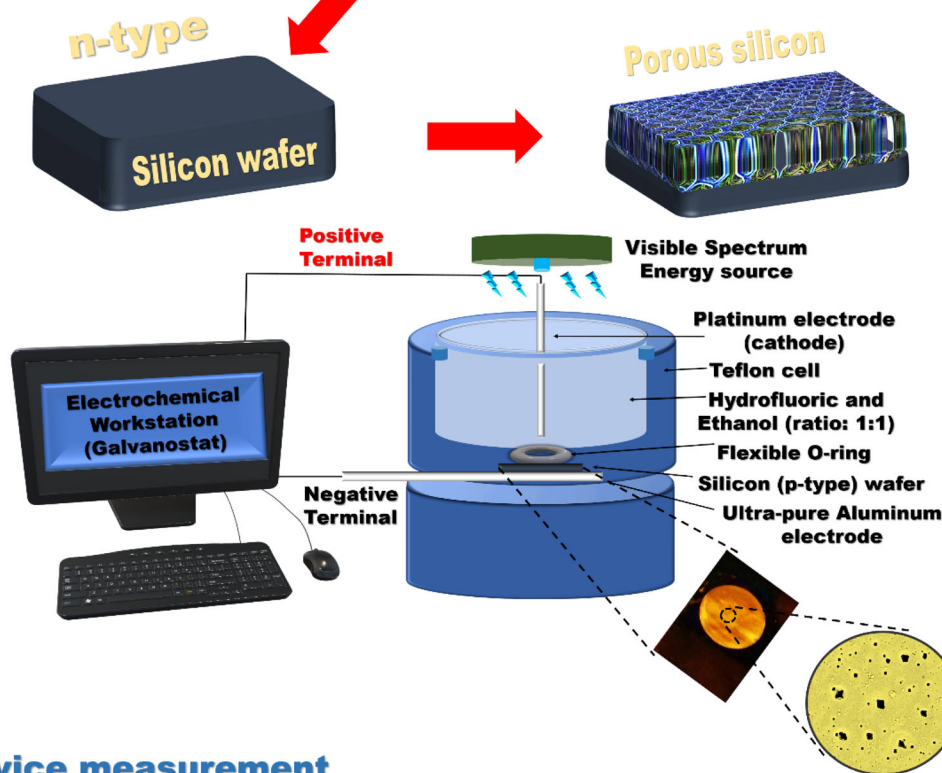
The Si surface underwent anodization in the course of the etching procedure. The electron-hole pairs in the Si were produced by external laser illumination. Since the rate of oxidation and the rate of Si breakdown were equal, constant pore development resulted. Surface hydrogen bonds were being chemically broken down and replaced by fluoride ions. When the circuit was open, the Si surface remained passivated. A hole (h^+) will consistently be created in order to establish a neutralized link Si-F. Si-F may form as a result of the F atom's preferred polarization activity with the Si atom when the anodic potential is precisely controlled. The Si atom receives a fresh F atom in a new place, leading to the formation of a hydrogen molecule (H_2) on its surface that could have been solubilized in an organic solvent like ethanol. The significant electronegativity of F atoms causes Si-Si connections to deteriorate when this approach is recurrent. The top of the Si wafer had Si atoms dissolved by HF acid, which made pits form more quickly [34]. In Fig. 2a, the surface morphologies of PS are depicted. It is evident that cavities are dispersed haphazardly over the surface. At decreasing depths, the PS appeared like a star and square shape. This pattern might be explained by a greater number of photo-initiated holes, which caused pore width to drop as depth grew. As a consequence, macropores with a steady critical current density were produced by maintaining critical current density at the bottom extremities of the cavities while increasing total current density as a consequence of the rise of electronic holes. The typical average pore size was calculated to be 250 nm. The pore size distribution profile is shown in Fig. 2b. FTIR was used to determine the surface bonds that were present, and the results showed that several bonds were formed, most notably the Si-F bond, which was caused by the HF solvent contributed during the electrochemical etching as shown in Fig. 2c. The P-Si samples' Raman spectra are displayed in Fig. 2d. The Raman spectra of PS samples had a widened peak centered at wavelengths 516.99, 519.26, and 519.29 cm^{-1} . A

1. Device fabrication

HF: Ethanol

+

Current



2. Device measurement

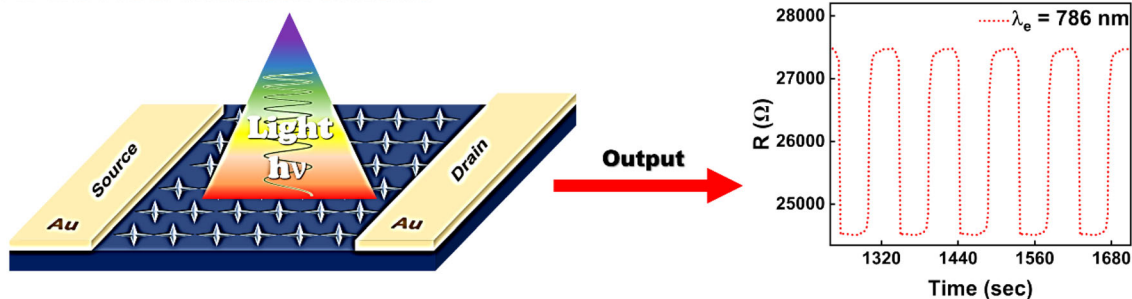


Fig. 1 A schematic representing electrochemical setup for device fabrication and its electrical measurement

shaded pink portion represents the standard silicon reference peak which is centered at 520 cm^{-1} . The peak displacement was brought about by the trapping of optical phonons, which established the existence of tiny Si crystallites within the pores [35]. Figure 2e depicts the PL spectrum of PS. It was discovered that the PL peak at 716.76 nm corresponded to a bandgap of 1.73 eV and for the bulk silicon the wavelength was $\sim 1110\text{ nm}$ with a corresponding bandgap of 1.12 eV . The PL peak in the porous silicon (PS) sample showed a blue shift which is associated with S-band emission from PS. The emission of light

in PS has been attributed to the quantum confinement effect in Si developed during the etching procedure. The quantum confinement hypothesis [36] offers a rationale for the blue shift. As per the hypothesis, PL emission from a band-band transition will be influenced by the dimensions of the Si crystallite in a manner that shifts the emission peak to a shorter wavelength considering the size/dimension at the nanoscale effect. Thus, the spectrum shift in our work is influenced by the size of the silicon porosity, and surface change distribution at the rim of the holes by spontaneous oxidation. Additionally, infrared

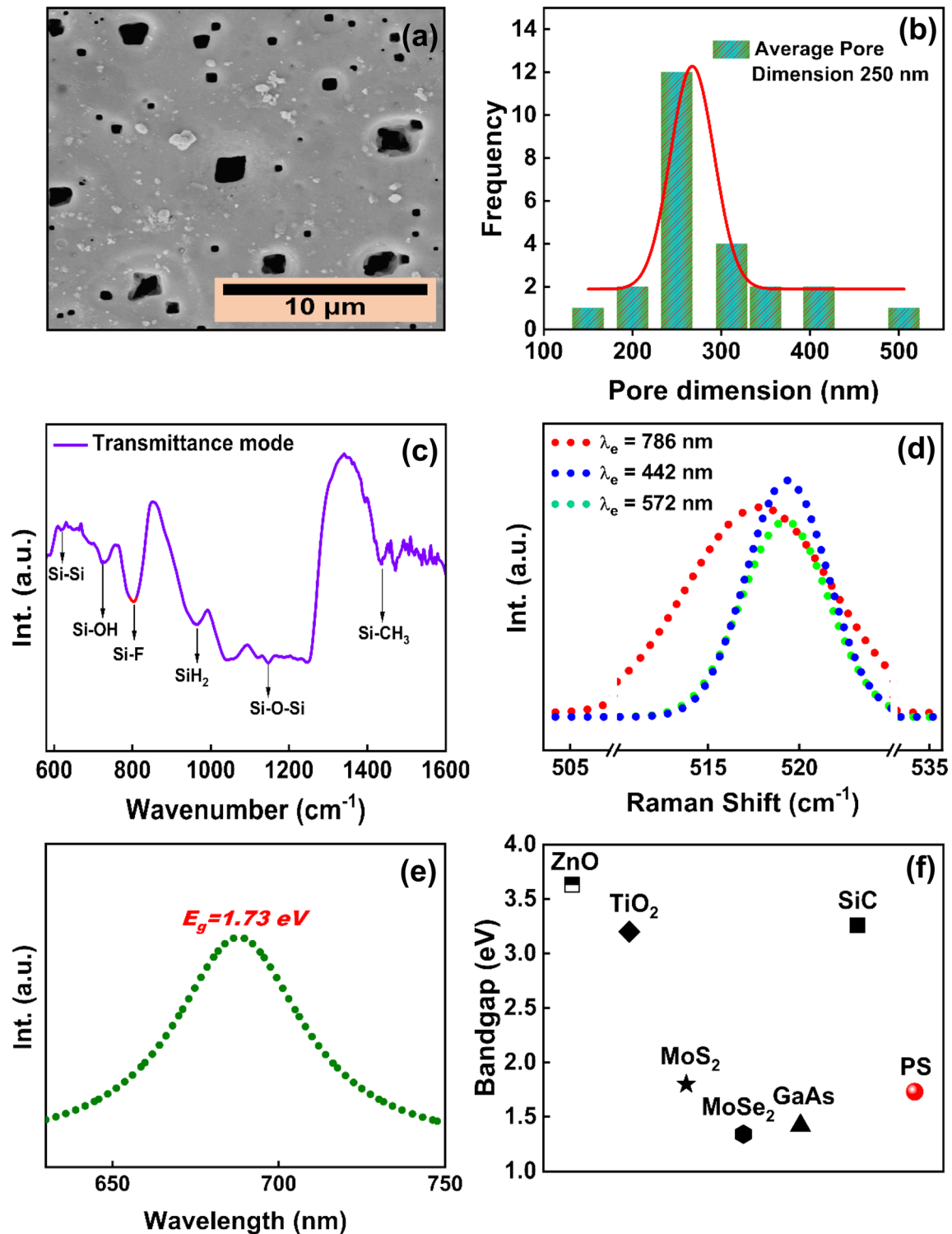


Fig. 2 The PS device **a** SEM image; **b** pore size distribution profile; **c** FTIR spectra; **d** Raman; and **e** PL. **f** Bandgap comparison

radiation is converted into visible light using the photoluminescence capabilities of PS. PS also has an intensely textured character. It will thus increase light trapping and decrease reflectance losses. The

bandgap comparison of other direct bandgap semiconductors with PS is shown in Fig. 2f. It was possible to measure photoresponse by maintaining a constant intensity of the incident light in aspects of

the variation in resistance for several light wavelengths, including 442, 572, 786, and 1065 nm, as illustrated in Fig. 3a–d. The resistance changes before and after illumination with respect to change in time in one complete cycle. The resistance changes before and after illumination are depicted as a plot of ΔR vs. wavelength in Fig. 3f. When exposed to 786 nm

wavelength radiation (red-light) highest sensitivity for the laser was found to be 11.18% (Fig. 3e), which is reasonable because the bandgap was estimated from the PL spectrum lies near the red-light region. Photoinduced electron-hole pairs are produced when the valence band (VB) electrons are switched to the conduction band (CB) in the presence of a light

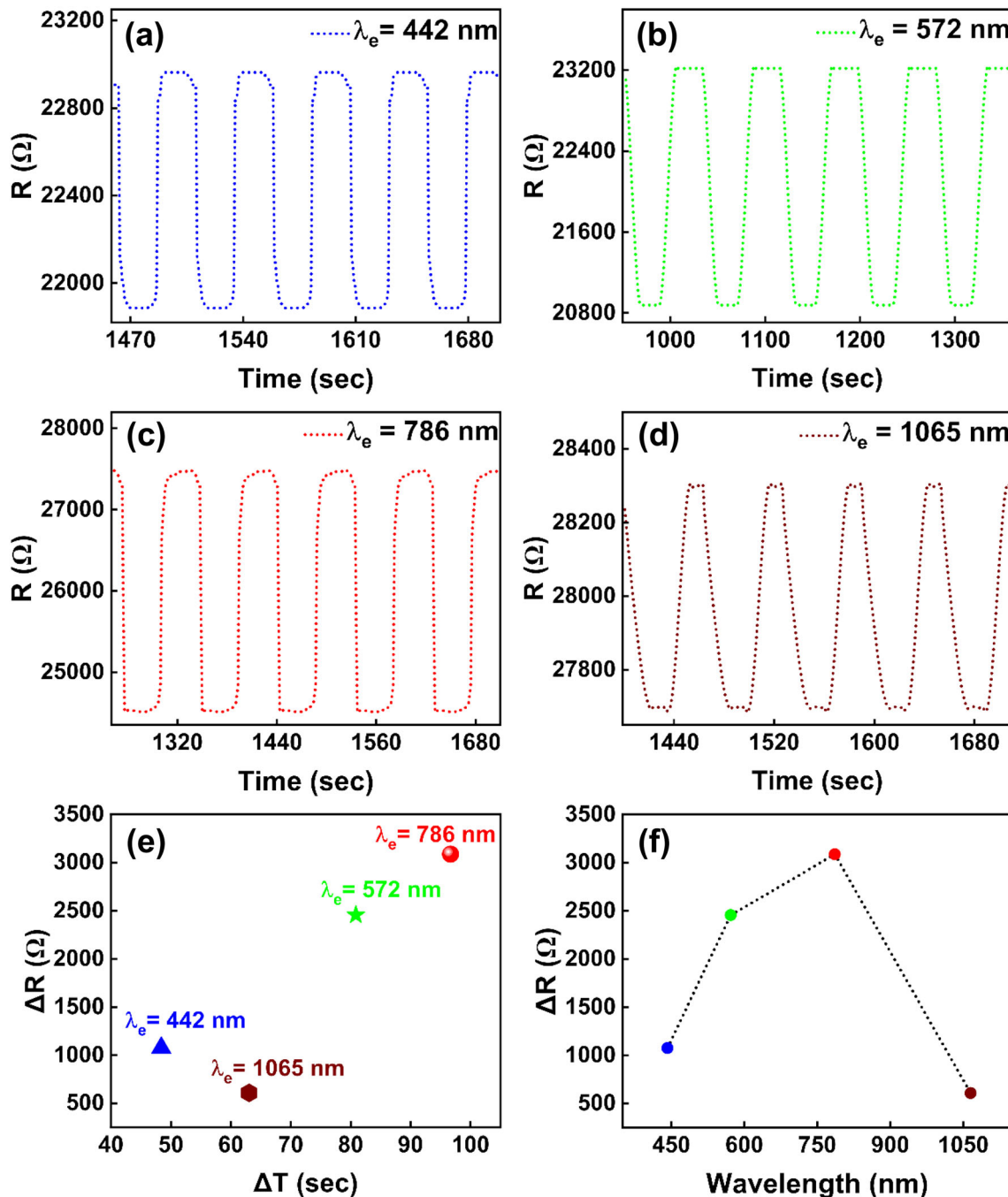


Fig. 3 PR of the PS device along with the different wavelengths: **a** 442 nm, **b** 572 nm, **c** 786 nm, **d** 1065 nm. Change in resistance before and after illumination (**e**) vs. change in time in one complete cycle; **f** at various wavelengths

source. As soon as the bias potential was supplied, the electrons began to migrate and sweep, completing the circuit and producing photogenerated-current (Fig. 4). When there is no laser illumination on the device surface, electrons migrate from the CB to the VB, where they recombine into electron-hole pairs.

4 Conclusion

The method we utilized in our research—anodization etching—was created to produce PS and is the most popular one. With the aid of external illumination, electrochemical etching was effectively used to create the n-type PS nanostructures. Unidirectional electrochemical etching was used to create pores with a mean size of 250 nm. Additionally, because of the quantum effect, the PL spectral data showed a hypsochromic shifting as a result. The sensitivity was discovered to be 11.18% when light with a wavelength of 786 nm was being used. This caused the bandgap to be adjusted from the infrared to the visible range. Thus, PS has the opportunity to be used for optical purposes in the visible region, especially in the red-light region. The sensitivity, selectivity, and stability of the material have been investigated through exposure to different wavelengths under

ambient conditions. The experimental work opens up the spectrum of the porous silicon-based photodetector in the field of optoelectronics by embedding sensors in the 786 nm range.

Acknowledgements

SA and AA are grateful to the Indian Institute of Technology Jodhpur, Rajasthan, India, for providing research facilities, infrastructure, and financial support. SA and AA would like to thank the Ministry of Human Resource Development for the financial support. The authors are thankful to Sprint Testing Solution and the Indian Institute of Technology Patna for providing a few characterization techniques facilities. PR would like to thank Science and Engineering Research Board for Start-up Research Grant (Grant nos. SRG/2022/000192, SRG/2022/000825, and SRG/2022/001377) for collaboration and Science for Equity Empowerment and Development Grant No. I/SEED/PRJ/20220044.

Author contributions

SA: Conceptualization, investigation, writing—original draft, and figure drawings, visualization reviewing, and editing. AA: Conceptualization, investigation, writing—original draft, figure drawings, visualization reviewing, and editing. MAS: Writing—original draft, and figure drawings. AK: Supervision, conceptualization, visualization—reviewing, and editing. PR: Supervision, conceptualization, visualization—reviewing, and editing.

Data availability

Not applicable.

Code availability

Not applicable.

Declarations

Conflict of interest The authors declare that they have no conflict of interest.

Ethical approval Not applicable.

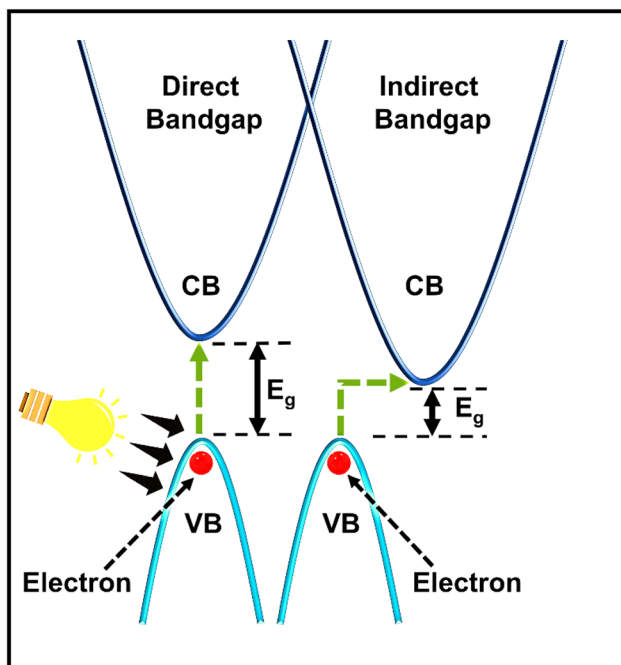


Fig. 4 The mechanism of direct and indirect transition of electron from VB to CB.

References

1. R. Moretta, L. De Stefano, M. Terracciano, I. Rea, Porous silicon optical devices: recent advances in biosensing applications. *Sensors* **21**, 1336 (2021)
2. W.G. Kreyling, M. Semmler-Behnke, Q. Chaudhry, A complementary definition of nanomaterial. *Nano Today* **5**, 165–168 (2010)
3. Y. Abdi, J. Derakhshandeh, P. Hashemi et al., Light-emitting nano-porous silicon structures fabricated using a plasma hydrogenation technique. *Mater. Sci. Eng. B* **124**, 483–487 (2005)
4. A. Uhler, Electrolytic shaping of germanium and silicon. *Bell Syst. Tech. J.* **35**, 333–347 (1956)
5. V. Torres-Costa, R.J. Martín-Palma, Application of nanostructured porous silicon in the field of optics. A review. *J. Mater. Sci.* **45**, 2823–2838 (2010)
6. J.-C. Lin, Y.-H. Lai, S.-H. Lu et al., Improvement of a capacitive UV-sensor by porous silicon powders embedded in epoxy on porous silicon film. *Opt. Mater. Express* **12**, 3143 (2022)
7. M.S. Choi, H.G. Na, A. Mirzaei et al., Room-temperature NO₂ sensor based on electrochemically etched porous silicon. *J. Alloys Compd.* **811**, 151975 (2019)
8. M.P. Stewart, J.M. Buriak, Chemical and biological applications of porous silicon technology. *Adv. Mater.* **12**, 859–869 (2000)
9. Y.-Y. Song, P. Schmuki, Modulated TiO₂ nanotube stacks and their use in interference sensors. *Electrochem. Commun.* **12**, 579–582 (2010)
10. W. Zhang, A. Farooq, W. Wang, Generating silicon nanoparticles using spark erosion by flushing high-pressure deionized water. *Mater. Manuf. Process.* **31**, 113–118 (2016)
11. M.A. Siddiqui, P. Jaiswal, Photocatalytic behavior of ferroelectric materials: comparative study of BaTiO₃ and Ag-loaded BaTiO₃ for wastewater treatment. *IOP Conf. Ser.: Mater. Sci. Eng.* **1166**, 012031 (2021)
12. Y. Zhang, J. Chen, L. Zhu, Z.L. Wang, Self-powered high-responsivity photodetectors enhanced by the pyro-phototronic effect based on a BaTiO₃/GaN Heterojunction. *Nano Lett.* **21**, 8808–8816 (2021)
13. G. Madhaiyan, T.-W. Tung, H.-W. Zan et al., UV-enhanced room-temperature ultrasensitive NO gas sensor with vertical channel nano-porous organic diodes. *Sens. Actuators B* **320**, 128392 (2020)
14. S. Ahmed, A. Ansari, A.S. Haidyrah et al., Hierarchical molecularly imprinted inverse Opal-Based platforms for highly selective and sensitive determination of histamine. *ACS Appl. Polym. Mater.* **4**, 2783–2793 (2022)
15. M. Imran, A.A. Chaudhary, S. Ahmed et al., Iron oxide nanoparticle-based ferro-nanofluids for advanced technological applications. *Molecules* **27**, 7931 (2022)
16. N. Hamdaoui, I. Ben Elkamel, A. Mezni et al., Highly efficient, low cost, and stable self-powered UV photodetector based on Co₂+:ZnO/Sn diluted magnetic semiconductor nanoparticles. *Ceram. Int.* **45**, 17729–17736 (2019)
17. A. Khan, S. Ahmed, B.-Y. Sun et al., Self-healable and anti-freezing ion conducting hydrogel-based artificial bioelectronic tongue sensing toward astringent and bitter tastes. *Biosens. Bioelectron.* **198**, 113811 (2022)
18. L. Mandal, N.S. Chaudhari, S. Ogale, Self-powered UV-vis photodetector based on ZnIn₂S₄/hydrogel interface. *ACS Appl. Mater. Interfaces* **5**, 9141–9147 (2013)
19. F. Akbar, M. Kolahdouz, S. Larimian et al., Graphene synthesis, characterization and its applications in nanophotonics, nanoelectronics, and nanosensing. *J. Mater. Sci.: Mater. Electron.* **26**, 4347–4379 (2015)
20. M. Kolahdouz, B. Xu, A.F. Nasiri et al., Carbon-related materials: graphene and carbon nanotubes in semiconductor applications and design. *Micromachines* **13**, 1257 (2022)
21. P. Ranjan, P. Tiwary, A.K. Chakraborty et al., Graphene oxide based free-standing films for humidity and hydrogen peroxide sensing. *J. Mater. Sci.: Mater. Electron.* **29**, 15946–15956 (2018)
22. A. Sinha, P. Ranjan, A.D. Thakur, Effect of characterization probes on the properties of graphene oxide and reduced graphene oxide. *Appl. Phys. A* **127**, 1–13 (2021)
23. P. Ranjan, V. Thomas, P. Kumar, 2D materials as a diagnostic platform for the detection and sensing of the SARS-CoV-2 virus: a bird's-eye view. *J. Mater. Chem. B* **9**, 4608–4619 (2021)
24. A. Khan, S.M. Islam, S. Ahmed et al., Direct CVD growth of graphene on technologically important dielectric and semiconducting substrates. *Adv. Sci.* **5**, 1800050 (2018)
25. A. Khan, J. Cong, R.R. Kumar et al., Chemical vapor deposition of graphene on self-limited SiC interfacial layers formed on silicon substrates for heterojunction devices. *ACS Appl. Nano Mater.* **5**, 17544 (2022)
26. J. Cong, A. Khan, P. Hang et al., Graphene/Si heterostructure with an organic interfacial layer for a self-powered photodetector with a high ON/OFF ratio. *ACS Appl. Electron. Mater.* **4**, 1715–1722 (2022)
27. J. Cong, A. Khan, J. Li et al., Direct growth of graphene nanowalls on silicon using plasma-enhanced atomic layer deposition for high-performance Si-based infrared photodetectors. *ACS Appl. Electron. Mater.* **3**, 5048–5058 (2021)
28. M. Imran, S. Ahmed, A.Z. Abdullah et al., Nanostructured material-based optical and electrochemical detection of

- amoxicillin antibiotic. *Luminescence* (2022). <https://doi.org/10.1002/bio.4408>
29. H.A. Hadi, R.A. Ismail, N.J. Almarshhadani, Preparation and characteristics study of polystyrene/porous silicon photodetector prepared by electrochemical etching. *J. Inorg. Organomet. Polym.* **29**, 1100–1110 (2019)
 30. C.W. Jang, D.H. Shin, S.-H. Choi, High-photoresponse and broad-band graphene/WS₂/Porous-Si heterostructure photodetectors. *ACS Appl. Nano Mater.* **5**, 13260–13266 (2022)
 31. I. Mal, S. Singh, D.P. Samajdar, Design and simulation of InAsBi PIN photodetector for Long wavelength Infrared applications. *Mater. Today: Proc.* **57**, 289–294 (2022)
 32. A. Kumar, P. Ranjan, Defects signature in VOC characterization of thin-film solar cells. *Sol. Energy* **220**, 35–42 (2021)
 33. S. Ahmed, S. Khatun, S. Sallam et al., Photoresponse of porous silicon for potential optical sensing. *EPL* **139**, 36001 (2022)
 34. C. Huo, J. Wang, H. Fu et al., Metal-assisted chemical etching of silicon in oxidizing HF solutions: origin, mechanism, development, and black silicon solar cell application. *Adv. Funct. Mater.* **30**, 2005744 (2020)
 35. M. Kadlečíková, J. Breza, L. Vančo et al., Raman spectroscopy of porous silicon substrates. *Optik* **174**, 347–353 (2018)
 36. M. Das, D. Sarkar, Morphological and optical properties of n-type porous silicon: effect of etching current density. *Bull. Mater. Sci.* **39**, 1671–1676 (2016)

Publisher's Note Springer Nature remains neutral with regard to jurisdictional claims in published maps and institutional affiliations.

Springer Nature or its licensor (e.g. a society or other partner) holds exclusive rights to this article under a publishing agreement with the author(s) or other rightsholder(s); author self-archiving of the accepted manuscript version of this article is solely governed by the terms of such publishing agreement and applicable law.